Supplementary Materials and Methods

Drosophila strains

A description of most of the genetic elements can be found at http://flybase.net (FlyBase Consortium, 1999). Drosophila stocks and crosses were kept under standard conditions. The following mutations were used: *shg*^{2}, *shg*^{119}, *baz*$^{815.8}$. FM7-*ftz-lacZ*, CyO-*wg-lacZ*, TM3-*ftz-lacZ*, or TM6-*Ubx-lacZ* blue balancers were used to identify homozygous embryos. The GAL4 system (Brand and Perrimon, 1993) was used for misexpression experiments. The epidermal *en*-GAL4 driver (A. Brand, Wellcome/CRC Institute, Cambridge, UK) and the tracheal *btl*-GAL4 driver (Shiga et al., 1996) were used at 29°C in combination with UAS-Spastin-GFP (Trotta et al., 2004), UAS-Spastin (our stock), UAS-EB1-GFP (Jankovics and Brunner, 2006), UAS-CD8-GFP, btl-RFP1-Moesin (Ribeiro et al., 2004) and at 18°C in combination with UAS-Rab11^{S25N} as Rab11 dominant negative and at 29°C in combination with UAS-Rab5^{S43N} as Rab5 dominant negative (both provided by Marcos González-Gaitán). The E-Cad-GFP has been described in (Huang et al., 2009) and the E-Cad-EosFP has been described in(Cavey et al., 2008).

Immunohistochemistry

Embryos were staged as described in (Campos-Ortega and Hartenstein, 1985) fixed and stained following standard protocols. To visualize MTs, embryos were fixed as previously described (Brodu et al., 2010). Embryos were heat-fixed and post-fixed in methanol for immunostaining using anti-Rab5 and anti-Rab11 antibodies (Miller et al., 1989). Primary antibodies were as described in (Brodu et al., 2010) with the following additions: anti-armadillo (1/500, DSHB), anti E-Cad (1/50, DSHB), anti-Crumbs (1/1000, U. Tepass), anti-Bazooka (1/2000, A. Wodarz), anti-Rab5 (1/50, M. Gonzalez-Gaitan); anti-Rab11 (1/100, BD Biosciences, #610656), anti-Nuf (1/1000, W. Sullivan;), anti-Uninflatable (Uif) (1/300, R. Ward;), anti-HRS (1/500, H. Bellen;). Secondary antibodies conjugated with Cy3, Cy5 (Jackson Laboratories) or Alexa Fluor 488, 546 and 647 (Life technologies) were used.

Live imaging

Embryos were processed as described in (Brodu et al., 2004). Imaging of EB1-GFP comets was carried out using a spinning disk 491 nm laser ×100/1.4 NA objective. Acquisition was every 1500 msec. Max intensity projection of Z stacks over 60 sec intervals are shown. EB1-GFP comets were observed in WT and Spastin overexpression contexts. For comparison, both

genetic contexts carried the same number of UAS transgenes so that the amount of GAL4 available to drive the UAS-EB1-GFP construct was identical.

Imaging of the tracheal development in absence of MTs was performed in embryos over-expressing Spastin-GFP in the tracheal system together with the expression of btl-mRFP-Moesin to highlight the tracheal apical domain (Ribeiro et al., 2004). Images were collected from stage 13-14 embryos on a Leica TCS SP5 confocal microscope with a ×63 oil immersion objective, 1.4 NA using the Leica TCS NT software. 30 sections spaced by 1µm were recorded every 5min. TIFF images were processed, with ImageJ.

Supplementary Movies

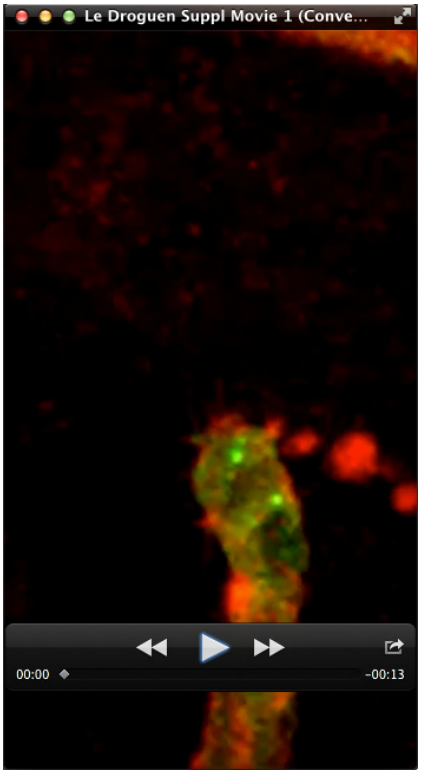

Supplementary Movie 1

Confocal life imaging of one DB expressing btl-RFP1-Moesin and UAS-spastin-GFP driven by btl-GAL4 during stages 14 to 15. Two channels, corresponding to spastin-GFP (green) and RFP-Moesin (red), were acquired simultaneously for better time resolution. Lateral views (z-stack maximum projections) were taken at 5 min intervals from stage 13 to 15. Anterior is to the left. Tracheal cell at the tip of the stalk gradually over-elongates, forming a long cytoplasmic thread. The following tracheal cells are under-elongated (white arrows).

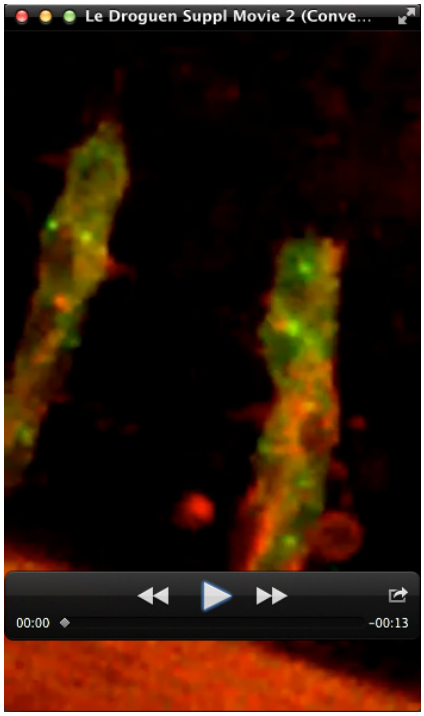

Supplementary Movie 2

Confocal life imaging of DB expressing btl-RFP1-Moesin and UAS-spastin-GFP driven by btl-GAL4 during stages 14 to 15. Two channels, corresponding to spastin-GFP (green) and RFP-Moesin (red), were acquired simultaneously for better time resolution. Lateral views (z-stack maximum projections) were taken at 5 min intervals from stage 13 to 15. Anterior is to the left. Tracheal cell at the base of the stalk gradually over-elongates, forming a long cytoplasmic thread (white arrow).

Supplementary Figures

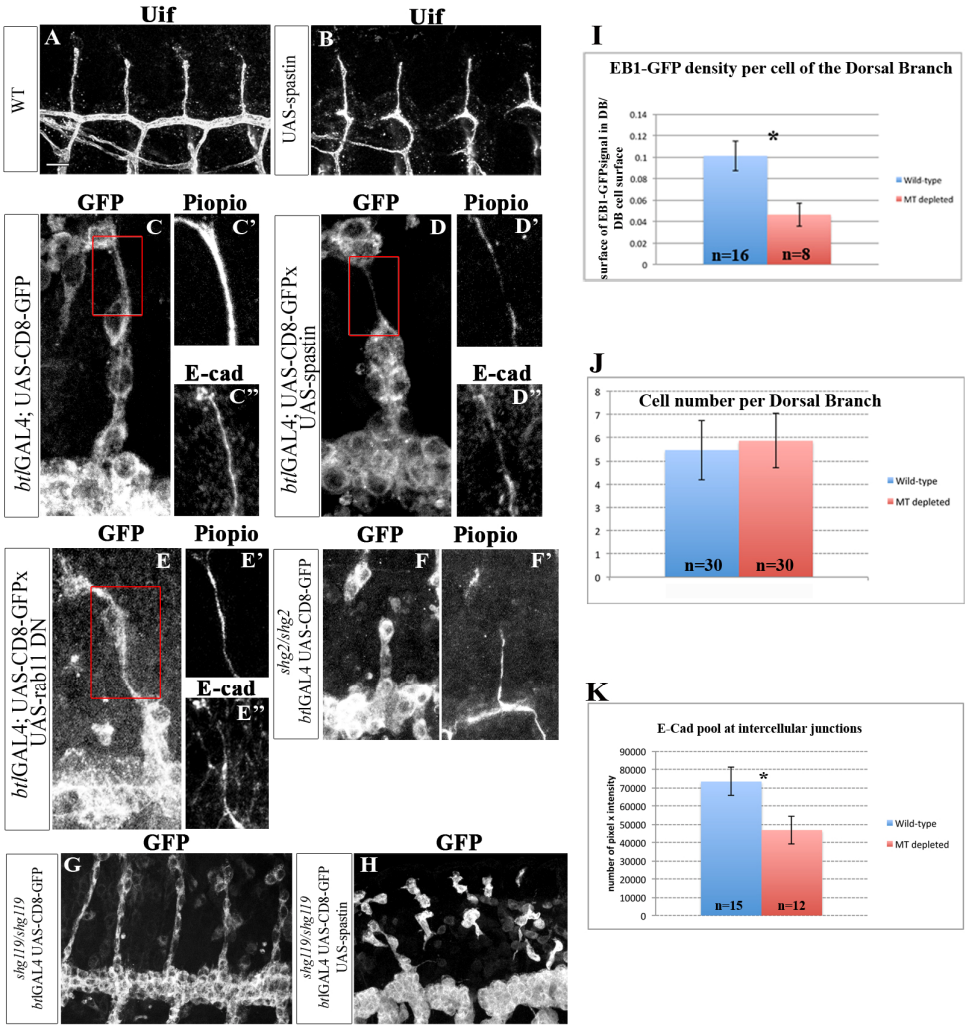

Supplementary Figure S1. MT depletion does not affect lumen deposition but interferes with E-Cad localisation and function

(A, B) Deposition of lumen products, revealed by the anti-Uninflatable (Uif) antibody, is similar in WT (A) and Spastin-overexpressing tracheal cells (B). Expression of the membrane bound form CD8::GFP in WT (C), MT-depleted (D) and Rab11DN overexpression contexts and of the corresponding distribution of the lumen product labelled with Piopio (C', D', E') and with E-Cad (C'', D'', E''). In the long cytoplasmic thread formed by an over-elongated cell, the lumen and the AJ are reduced and irregular. (F, F') Expression of the membrane bound form CD8::GFP in mutant embryos for the amorphic allele shg^{2} (F). The lumen labelled with Piopio (F') is irregular. (G, H) Tracheal branch outgrowth in homozygous mutant embryos for the hypomorphic allele shg^{119} alone (G) or associated with Spastin

overexpression (H). (I) Graph plotting the quantification of the EB1-GFP signal density in WT and MT-depleted tracheal cells of the DB. p-value Test Mann-Whitney = 0.016. (J) At stage 15, cell numbers in DBs of central metameres A4 to A7 are comparable between WT and MT-depleted embryos (K) Graph showing the quantifications, in WT and MT-depleted contexts, of E-Cad immunofluorescence restricted to intercellular junctions of the DB at stage 16; p-value test Mann-Whitney = 0.019.

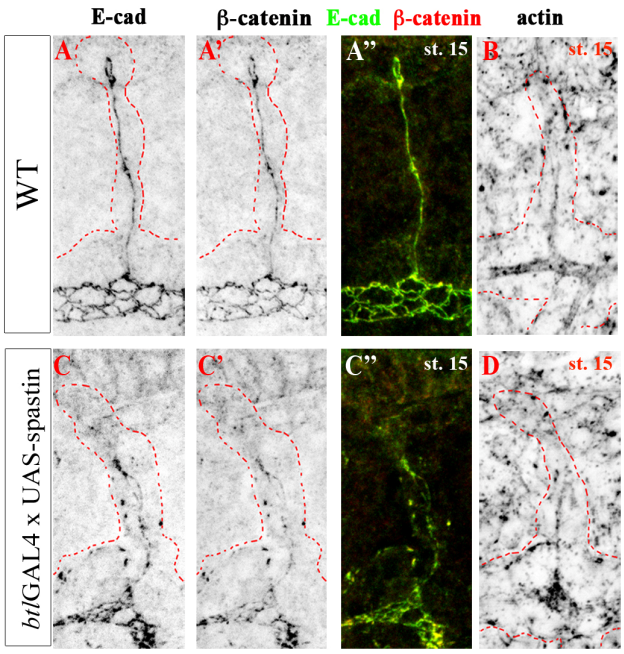

Supplementary Figure S2. Characterisation of E-Cad intracellular accumulation in MT-depleted tracheal cells

(A-D) DT and DB of stage 15 embryos in WT (A, B) or Spastin overexpression (C, D) contexts. MT depletion induces cytoplasmic accumulation of AJ components as shown using E-Cad and β-catenin antibodies (compare A', A'' to B, B'') but does not significantly alter the apical localisation of actin (compare B to D). E-Cad distribution in WT (E) and Spastin overexpressing (F) embryos at stage 14 is presented. MT depletion produces cytoplasmic accumulation of E-Cad (F).

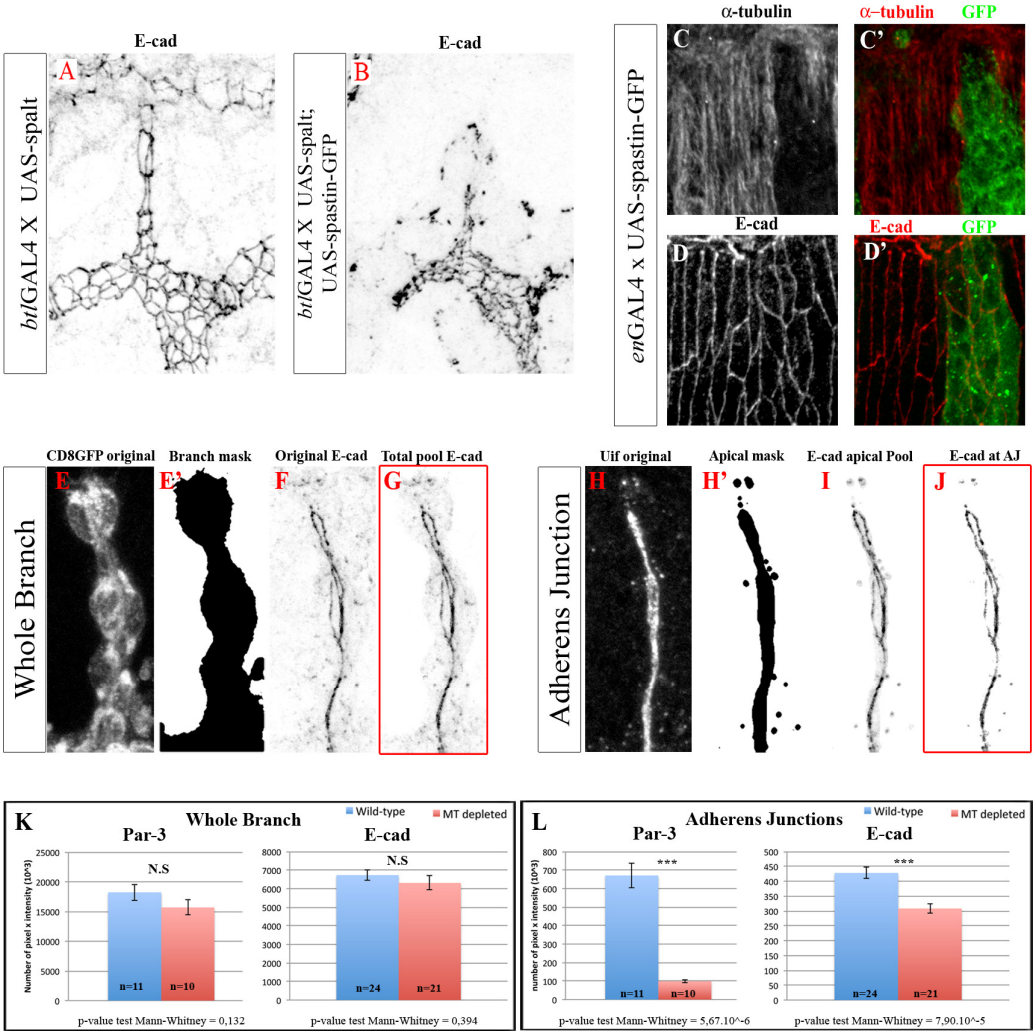

Supplementary Figure S3. MT depletion does not depend on the intercalation state and has no influence on epidermal cells. Details of the macro developed to quantify AJ component levels in tracheal cells

(A) Overexpression of the Spalt transcription factor prevents tracheal cell intercalation as observed by E-Cad staining. Together with Spastin overexpression (B), cell intercalation is still prevented and cytoplasmic accumulation of E-Cad is visible. (C-D') Spastin overexpression in the dorsal part of ectodermal cells using the *en*-GAL4 driver. As in trachea, strong depolymerisation of MTs is observed (C, C') in stage 15 embryos. However, as opposed to trachea, E-Cad distribution is not altered (D, D'). (E-J) The series of pictures extracted from image processing depict how the macro functions using ImageJ. Z-projections are represented but the macro processes the images section by section. First, the macro is programmed to define the contours of CD8-GFP expression in tracheal cells (E) thus defining

a branch mask (E'). Within this branch mask, the total pool of E-Cad (F, G) is measured and corresponds to the number of pixels multiplied by their intensity. Second, the macro is programmed to define a mask outlining the luminal staining Uif (H) and corresponding to the apical domain of tracheal cells (H'). This apical mask is again applied on the E-Cad staining to extract part of the E-Cad corresponding to the apical pool (I). Finally, the apical pool of E-Cad is determined using as cut-off the mean intensity value of WT AJ staining. This pool of E-Cad at the AJ (J) corresponds to the number of remaining pixels multiplied by their intensity. The same process is used for Par-3 staining and for both in WT and MT-depleted contexts. (K, L) Graphs showing the quantifications of Par-3 and E-Cad immunofluorescence in WT and MT-depleted contexts within the entire DT (K), or restricted to AJs (L).

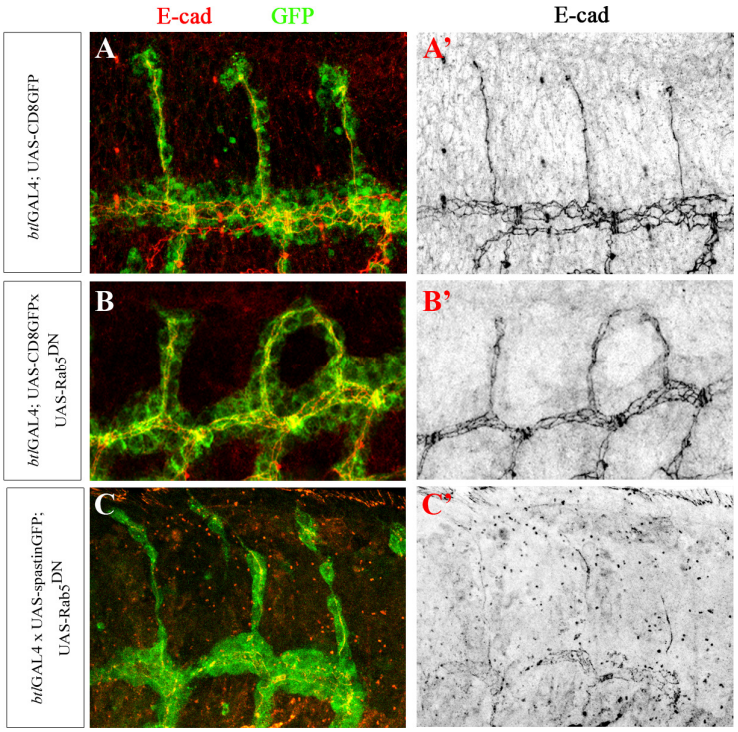

Supplementary Figure S4. Blocking E-Cad internalisation by overexpressing Rab5DN does not prevent trachea cell over-elongation induced by the absence of MTs

Stage 15 embryos expressing the membrane-bound form CD8::GFP (A-C) in tracheal cells and E-Cad localisation (A'-C'). Overexpression of Rab5DN inhibits intercalation in the DB visualized as parallel lines of E-cad (B') compared to a straight line formed by autocellular junctions in controls (A'). Overexpression of Rab5DN in cells depleted of MTs leads to cell over-elongation and branch breaks (C) as in overexpression of Spastin alone. A strong reduction of E-Cad levels at AJs is also observed (C').

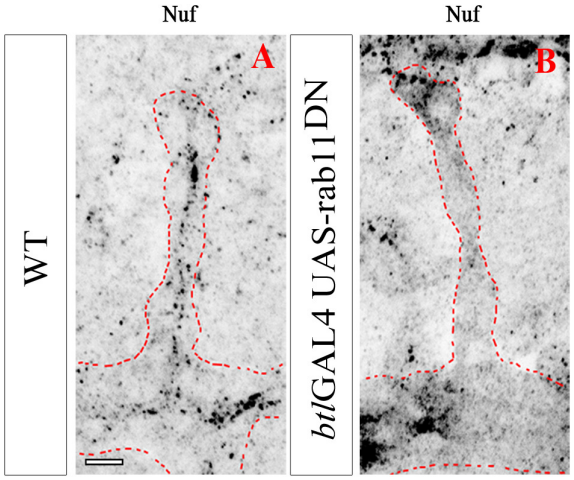

Supplementary Figure S5. Overexpression of Rab11-DN disrupts apical recycling endosome distribution in tracheal cells

Nuf-positive recycling endosomes accumulate apically in the DT and DB at stage 15 of WT embryos (A). Overexpression of Rab11-DN in tracheal cells disrupts recycling endosome distribution (B).

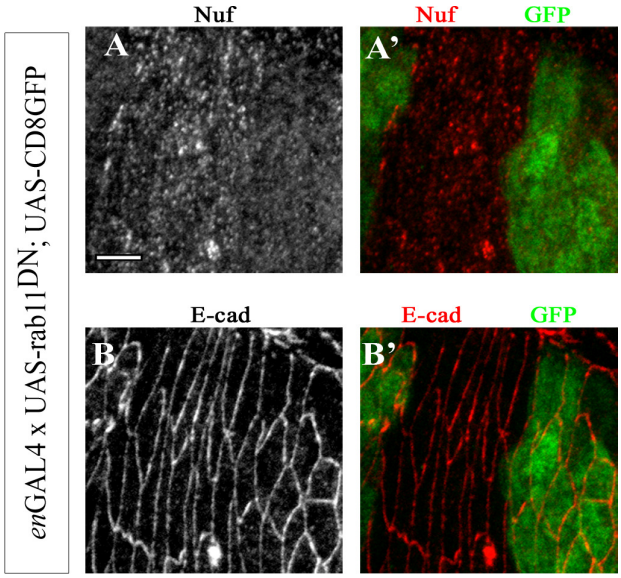

Supplementary Figure S6. Overexpression of Rab11-DN in ectodermal cells affects the distribution of recycling endosomes but not of E-Cad.

Overexpression of Rab11-DN driven by *en*-GAL4 in ectodermal cells of the dorsal side of stage 15 embryos. As in tracheal cells, spreading of Nuf-positive recycling endosomes is observed (A-A'), but as opposed to tracheal cells, E-Cad distribution is not altered (B-B').

Supplementary References

Brand, A. H. and Perrimon, N. (1993) 'Targeted gene expression as a means of altering cell fates and generating dominant phenotypes', *Development* 118(2): 401-15.

Brodu, V., Baffet, A. D., Le Droguen, P.-M., Casanova, J. and Guichet, A. (2010) 'A developmentally regulated two-step process generates a noncentrosomal microtubule network in Drosophila tracheal cells', *Dev Cell* 18(5): 790-801.

Brodu, V., Elstob, P. R. and Gould, A. P. (2004) 'EGF receptor signaling regulates pulses of cell delamination from the Drosophila ectoderm', *Dev Cell* 7(6): 885-95.

Campos-Ortega, A. J. and Hartenstein, V. (1985) *The embryonic development of Drosophila melanogaster*: Springer-Verlag, New York.

Cavey, M., Rauzi, M., Lenne, P.-F. and Lecuit, T. (2008) 'A two-tiered mechanism for stabilization and immobilization of E-cadherin', *Nature* 453(7196): 751-6.

Huang, J., Zhou, W., Dong, W., Watson, A. M. and Hong, Y. (2009) 'From the Cover: Directed, efficient, and versatile modifications of the Drosophila genome by genomic engineering', *Proc Natl Acad Sci USA* 106(20): 8284-9.

Jankovics, F. and Brunner, D. (2006) 'Transiently reorganized microtubules are essential for zippering during dorsal closure in Drosophila melanogaster', *Dev Cell* 11(3): 375-85.

Miller, K. G., Field, C. M. and Alberts, B. M. (1989) 'Actin-binding proteins from Drosophila embryos: a complex network of interacting proteins detected by F-actin affinity chromatography', *J Cell Biol* 109(6 Pt 1): 2963-75.

Ribeiro, C., Neumann, M. and Affolter, M. (2004) 'Genetic control of cell intercalation during tracheal morphogenesis in Drosophila', *Current biology : CB* 14(24): 2197-207.

Shiga, Y., Tanaka-Matakatsu, M. and Hayashi, S. (1996) 'A nuclear GFP/β-galactosidase fusion protein as a marker for morphogenesis in living *Drosophila*', *Develop. Growth Differ.* 38: 99-106.

Trotta, N., Orso, G., Rossetto, M. G., Daga, A. and Broadie, K. (2004) 'The hereditary spastic paraplegia gene, spastin, regulates microtubule stability to modulate synaptic structure and function', *Current biology : CB* 14(13): 1135-47.